Degradacija kvazi-2D perovskita: nagovještaji izračunima iz prvih principa

Đudarić, Dino

Master's thesis / Diplomski rad

2022

Degree Grantor / Ustanova koja je dodijelila akademski / stručni stupanj: **University of Zagreb, Faculty of Science / Sveučilište u Zagrebu, Prirodoslovno-matematički fakultet**

Permanent link / Trajna poveznica: https://urn.nsk.hr/urn:nbn:hr:217:343114

UNIVERSITY OF ZAGREB
FACULTY OF SCIENCE
DEPARTMENT OF PHYSICS

Dino Đudarić

DEGRADATION OF QUASI-2D PEROVSKITES: HINTS FROM FIRST-PRINCIPLES CALCULATIONS

Master Thesis

Zagreb, 2022

SVEUČILIŠTE U ZAGREBU
PRIRODOSLOVNO-MATEMATIČKI FAKULTET
FIZIČKI ODSJEK

Dino Đudarić

DEGRADACIJA KVAZI-2D PEROVSKITA: NAGOVJEŠTAJI IZRAČUNIMA IZ PRVIH PRINCIPA

Diplomski rad

Zagreb, 2022.

UNIVERSITY OF ZAGREB
FACULTY OF SCIENCE
DEPARTMENT OF PHYSICS

INTEGRATED UNDERGRADUATE AND GRADUATE UNIVERSITY
PROGRAMME IN PHYSICS

Dino Đudarić

Master Thesis

Degradation of quasi-2D perovskites: hints from first-principles calculations

Advisor: Luca Grisanti, dr. sc.

Co-Advisor: Damjan Pelc, doc. dr. sc.

Master Thesis grade: _____

Committee: 1. _____

2. _____

3. _____

Master Thesis defence date: _____

Zagreb, 2022

I would like the thank my advisor dr. sc. Luca Grisanti and doctorand Juraj Ovčar for all the help with this thesis.
Također se zahvaljujem obitelji i prijateljima na podršci tijekom cijelog studija.

Degradacija kvazi-2D perovskita: nagovještaji izračunima iz prvih principa

Sažetak

Predmet ovog diplomskog rada je proučavanje degradacije kvazi-2D perovskita BA_2PbI_4 u prisutnosti kisika i svjetlosti u okviru teorije funkcionala gustoće. Energije vezanja kisika na (001) i (110) površine kvazi-2D BA_2PbI_4 perovskita izračunate su koristeći geometrijsku optimizaciju. Za (001) površinu, dobivena je ovisnost energija vezanja o z koordinati kisika kada je kisik postavljen iznad joda. Za (110) površinu dobivena je ovisnost energija vezanja o x i y koordinate kisika. Energija prijenosa elektrona je također izračunata koristeći ograničenu teoriju funkcionala gustoće. Rezultati pokazuju slabu adsorpciju neutralnog kisika kao i mogućnost degradacije svjetloću potpomognutim stvaranjem superoksida.

Ključne riječi: perovskit, teorija funkcionala gustoće, površina, kisik, energija vezanja, energija prijenosa elektrona

Degradation of quasi-2D perovskites: hints from first-principles calculations

Abstract

The topic of this master thesis is the study of degradation of quasi-2D perovskite BA_2PbI_4 in the presence of oxygen and light using density functional theory. Binding energies of oxygen to (001) and (110) surface of quasi-2D BA_2PbI_4 perovskite are calculated using geometry optimisation. For (001) surface, we obtain the dependence of binding energy on the z coordinate of oxygen when placed above an iodine atom. For (110) surface, we obtain x and y oxygen coordinate dependence of binding energy. The electron transfer energy is also calculated with the use of constrained density functional theory. The results show weak adsorption of neutral oxygen as well as the possibility of degradation by light-assisted generation of superoxide.

Keywords: perovskite, density functional theory, surface, oxygen, binding energy, electron transfer energy

Contents

1 Introduction

Hybrid inorganic-organic halide perovskite are a promising class of materials for development of low-cost optoelectronic devices such as solar cells, light-emitting diodes and lasers. Solar cell applications in particular have generated intense interest in recent years due to the rapid rise in power conversion efficiencies of up to 22% for perovskite photovoltaics [1]. Perovskite materials share similar structural features with the namesake mineral $CaTiO_3$. The structure of methylammonium lead iodide, $CH_3NH_3PbI_3$ (or $MAPbI_3$) is shown in Figure 1.1. As can be seen, the methylammonium cation ($CH_3NH_3^+$) occupies the central site surrounded by 12 nearest-neighbour iodide ions in corner-sharing PbI_6 octahedra. Many interesting properties of halide perovskites derive from their soft lattices and dynamically disordered crystal structure, which favorably modifies their charge-carrier recombination lifetimes [2]. However, a major obstacle in further development exists in the form of limited composition accessibility in the ABX_3 (A = Cs^+, $CH_3NH_3^+$, $[HC(NH_2)_2]^+$; B = Pb^{2+}, Ge^{2+}, Sn^{2+}; X = Cl^-, Br^-, I^-) perovskite structure, with only three A-site cations being able to maintain the 3D corner-sharing inorganic framework, in some cases forming only metastable compounds. A solution to this compositional diversity was found in the form of two-dimensional halide perovskites [2].

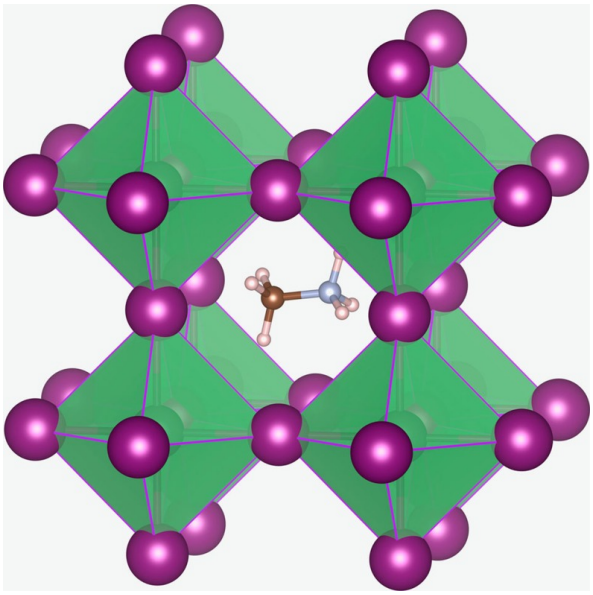

Figure 1.1: Structure of 3D perovskite $MAPbI_3$. [3]

2D perovskites obtained through chemical dimensional reduction of 3D crystal lattice, $(A')_m(A)_{n-1}B_nX_{3n+1}$, adopt a new structural and compositional degrees of

freedom, where monovalent (m = 2) or divalent (m = 1) A' cations can intercalate between the 2D perovskite sheets. This leads to a large variety of hybrid organic-inorganic materials with tailorable functionalities but also gives rise to an unparalleled structural complexity which allows for fine-tuning of the optoelectronic properties.

The diversity of 2D perovskites comes from two key components: the inorganic layers and their modifications, and the organic cation diversity. As the two heterogeneous components blend, either by synthetic manipulation (shuffling the organic cations or inorganic elements) or by application of external stimuli (temperature and pressure), the modular perovskite structure evolves to form crystallographically defined quantum wells. The complex electronic structure that arises is sensitive to the structural features that could be in turn used as a knob to control the dielectric and optical properties of the quantum wells. In the 2D hybrid halide perovskites, the organic spacers act as insulating barriers that confine the charge carriers in two dimensions, but they also serve as dielectric moderators that determine the electrostatic forces exerted on the photogenerated electron-hole pairs [2]. Figure 1.2 shows the structure of 2D perovskites with different number of layers n and their comparison to the 3D perovskite structures. 3D perovskite structure is obtained as the limit $n \to \infty$ of a 2D perovskite structure.

Before halide perovskites can be successfully used in commercial solar cell applications, long-term stability needs to be studied. It has been generally observed that external conditions such as moisture, elevated temperature, oxygen and UV radiation cause device instability at higher rates than those typically observed in polymer and dye-sensitized photovoltaics. Specifically, it has been demonstrated [4] that exposure of $CH_3NH_3PbI_3$ photoactive layers to light and oxygen leads to the formation of superoxide (O_2^-) species. This reactive (O_2^-) species can deprotonate the methylammonim cation ($CH_3NH_3PbI_3^*$), leading to the formation of PbI_2, water, methylamine and iodine. Photo-oxidative degradation of $CH_3NH_3PbI_3$ was also studied from first-principles calculations in [5] where further insight into mechanism and solutions was provided. Another study [6] using first-principles investigated effect of water and defects on this degradation process. Possible solution to stability issues would be the use of 2D perovskites with similar power conversion efficiencies.

In this work we have employed computational methods based on density func-

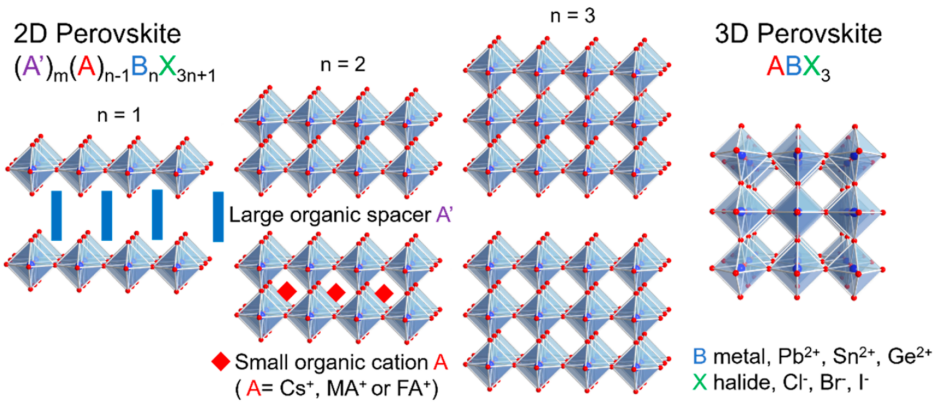

Figure 1.2: Shematic illustration of the evolution from a 2D perovskite to a 3D perovskite structure [2].

tional theory to investigate oxygen adsorption to surfaces of quasi-2D perovskite butylammonium lead iodide ($CH_3(CH_2)_3NH_3)_2PbI_4$ (BA_2PbI_4) which is a monovalent single layer 2D perovskite. Using constrained density functional theory we have also investigated electron transfer from the surface to the oxygen molecule which simulates creation of reactive superoxide.

2 Methods

2.1 Density functional theory

Density functional theory (DFT) was originally formulated in two works: Hohenberg and Kohn provided the theoretical background [7], followed by work by Kohn and Sham containing the directions for DFT calculations [8]. The key theoretical concepts are developed around the idea that the external potential U in which particles are moving is uniquely determined (up to a constant) by the density of particles $n(\vec{r})$ in the ground state; the system energy $E[n]$ is a functional of particle density $n(\vec{r})$, while the ground state energy is a global minimum of this functional, and particle density of this global minimum is the ground state particle density [7]. The exact particle density of the system, $n(\vec{r})$, can be viewed as the particle density of a fictitious system (the "Kohn-Sham system") of non-interacting particles [8]. Besides, any Kohn-Sham non-interacting particle is moving in a nonlocal Kohn-Sham potential, V_{KS}, which has multiple contributions: U (external potential), V_H (Hartree potential, elecrostatic potential of the electron charge density) and V_{xc} (exchange-correlation potential). V_{xc}, generally a nonlocal contribution, is the most critical part of density functional theory as its exact form is unknown so various approximations are used. For the exchange part of V_{xc}, Hartree-Fock exchange gives exact values, however, since it is a nonlocal contribution, it is numerically too demanding and therefore replaced by approximations such as Dirac LDA (local density approximation), GGA (generalized gradient approximation), hybrid potential (mix of HF and local potentials), etc. For the correlation part of V_{xc}, approximations are constructed by interpolating analytical calculations (perturbation theory) and adjusting numerical results that are outside the Hartree-Fock approximation. One example of correlation energy is the Wigner formula which is obtained by interpolating between random phase approximation results in the high density limit and Wigner lattice in the low density limit.

A Schrödinger-like equation for Kohn-Sham particles can be obtained:

$$\left[-\frac{\hbar^2}{2m}\vec{\nabla}^2 + U(\vec{r}) + V_H(\vec{r})\right]\psi_m(\vec{r}) + \int d\vec{r'} V_{xc}(\vec{r'},\vec{r})\psi_m(\vec{r'}) = e_m\psi_m(\vec{r}) \tag{2.1}$$

which is a system of 3-dimensional partial differential equation. By solving this system of equations, the density of Kohn-Sham particles in the ground state can be

calculated from the wave functions:

$$n(\vec{r}) = \sum_{n \in \text{occ.}} |\psi_n(\vec{r})|^2, \tag{2.2}$$

where the sum is performed over occupied states only. The Kohn-Sham potential depends on particle density, so potentials, density and wave functions need to be calculated self-consistently. Minimizing the ground state energy functional with respect to the Kohn-Sham charge density $n(\vec{r})$ yields the exact charge density, ground state energy and other ground-state observables of the physical system.

2.2 Gaussian and plane wave approach in the implementation of DFT codes

In standard DFT codes for solid state physics, wave functions are expanded in the plane wave (PW) basis. The periodic part of Bloch wave function is represented by a Fourier series of reciprocal lattice vectors. Considering numerical restrictions, the Fourier series is truncated at sufficiently high wave numbers. Then, solving the Kohn-Sham equation comes down to determining the eigenvalues of matrix with eigenvectors built from the Fourier components of wave functions. This approach does not scale really well with system size so other approaches which offer various optimisation algorithms are used.

All DFT calculations in this work are carried out using CP2K (version 8.2) [9]. CP2K is an open source electronic structure and molecular dynamics software package used to perform atomistic simulations of solid-state, liquid, molecular and biological systems. It is especially aimed at massively parallel and linear-scaling electronic structure methods and state of the art ab initio molecular dynamics simulations. DFT approach used in CP2K's electronic structure module *Quickstep* is the Gaussian and plane wave approach (GPW). In the GPW approach a contracted Gaussian basis set $g\left(\vec{r}\right)$ is used to expand wave functions

$$\phi\left(\vec{r}\right) = \sum_{u} d_u g_u\left(\vec{r}\right) \tag{2.3}$$

where the contracted coefficients d_u are fixed and the primitive Gaussians

$$g\left(\vec{r}\right) = r^l \exp\left[-\alpha\left(\vec{r}-\vec{A}\right)^2\right] Y_{lm}\left(\vec{r}-\vec{A}\right) \tag{2.4}$$

are centered at atomic positions. These functions are defined by the exponent α, the spherical harmonics Y_{lm}, with angular momentum (l, m) and the coordinates of their center $\vec{A}$. In CP2K, unique properties of Gaussians such as analytic integration and the product theorem are exploited. Another important property is that the Fourier transform of a Gaussian is again a Gaussian function:

$$\int \exp\left[-\alpha\vec{r}^2\right] \exp\left[-i\vec{G}\cdot\vec{r}\right] d\vec{r} = \exp\left[-\frac{\vec{G}^2}{4\alpha}\right] \tag{2.5}$$

This property is directly connected with the fact that integration of Gaussian functions on equidistant grids shows exponential convergence with grid spacing. In order to take advantage of this property a set of equidistant grid points is defined within a computational box or periodic unit cell. Any function with periodicity given by the lattice vector and defined on the real-space points can be transformed into reciprocal space representation by the Fourier transform

$$f(\vec{G}) = \sum_{\vec{R}} f(\vec{R}) \exp[i\vec{G}\cdot\vec{R}] \tag{2.6}$$

The accuracy of this expansion is given by the grid spacings or the PW cutoff defining the largest vector $\vec{G}$ included in the sum.

In the Kohn-Sham method, the electron density is defined by

$$n(\vec{r}) = \sum_{\mu\nu} P_{\mu\nu}\phi_\mu(\vec{r})\phi_\nu(\vec{r}) \tag{2.7}$$

where the density matrix $\boldsymbol{P}$, with elements $P_{\mu\nu} = \sum_i f_i c_{\mu i} c_{\nu i}$ is calculated from the orbital occupations f_i and the orbital expansion coefficients $c_{\mu i}$ of the common linear combination of atomic orbitals $\Phi_i(\vec{r}) = \sum_\mu c_{\mu i}\phi_\mu(\vec{r})$. Therein, $\Phi_i(\vec{r})$ are the so-called molecular orbitals (MOs) and $\phi_\mu(\vec{r})$ are the atomic orbitals (AOs). In the PW expan-

sion, however, the density is given by

$$n(\vec{r}) = \sum_{\vec{G}} n(\vec{G}) \exp[i\vec{G} \cdot \vec{r}] \tag{2.8}$$

The definitions given above allow us to calculate the expansion coefficients $n(\vec{G})$ from the density matrix $P_{\mu\nu}$ and the basis functions $\phi_\mu(\vec{r})$. The dual representation of the density is used in the definition of the GPW-based KS energy expression

$$E[\mathbf{P}] = E^{kin}[\mathbf{P}] + E^{ext}[\mathbf{P}] + E^{ES}[n_{\vec{G}}] + E^{XC}[n_{\vec{G}}] \tag{2.9}$$

to facilitate efficient and accurate algorithms for electrostatic as well as exchange and correlation energies. The efficient mapping $P_{\mu\nu} \rightarrow n(\vec{G})$ is achieved by using multi-grid methods, optimal screening in real-space, and the separability of Cartesian Gaussian functions in orthogonal coordinates. *Quickstep* uses a multi-grid system for mapping the product Gaussians onto the real-space grid(s), so that wide and smooth Gaussian functions are mapped onto a coarser grid than narrow and sharp Gaussians. The electron density is always mapped onto the finest grid. Details on the *orbital transformation* (OT) method which was used with *direct inversion in the iterative subspace* (DIIS) minimization can be found in references [10] and [11].

2.3 Pseudopotentials

In order to simplify calculations the problem of movement of all electrons is simplified by considering only valence electrons (outer shell electrons). The Kohn-Sham potential coming from core with inner electrons is replaced with an effective potential referred to as pseudopotential. CP2K also employs the use of pseudopotentials to describe inner shells. This is done to reduce basis set size and to reduce number of electron which leads to an effective speedup of calculations. The use of pseudopotentials in the GPW method also requires the use of a correspondingly adapted basis sets. Pseudopotentials used in our calculations are GTH-PBE [12] where GTH stands for Goedecker-Teter-Hutter and PBE stands for Perdew-Burke-Ernzerhof. The former are authors of Gaussian pseudopotentials and the latter are authors of the functional used to generate these pseudopotentials. Basis sets are molecularly optimised basis sets refered as TZV2P-MOLOPT-GTH [13]; the first part of the name is a label for

triple-zeta valence, i.e. three contracted functions per orbital plus two sets of polarisation functions with $l = l_{\max} + 1$, the second part is the name of the basis and the last part refers to the fact that this basis is adapted for GTH pseudopotential.

2.4 Constrained DFT

In addition, we carried out constrained DFT (CDFT) calculations where an oxygen molecule was constrained to be negatively charged while the whole structure was kept neutral, simulating an electron transfer from the surface to the oxygen.

In CDFT, charge and spin localized states are created by enforcing electron and spin density localization within atom centered regions of space. The relevant theory has been derived by Wu and Van Voorhis [14, 15]. To summarize, the charge/spin localized states can be generated by augmenting the Kohn-Sham energy functional by additional constraint potentials

$$E_{CDFT}\left[n(\vec{r}), \vec{\lambda}\right] = \max_{\vec{\lambda}} \min_{n(\vec{r})} \left(E_{KS}\left[n(\vec{r})\right] + \sum_{c} \lambda_c \left[\sum_{i=\uparrow,\downarrow} \int w_c^i(\vec{r}) n^i(\vec{r}) d\vec{r} - N_c \right] \right) \tag{2.10}$$

where $\vec{\lambda} = [\lambda_1, \lambda_2, ...]^T$ are constraint Lagrangian multipliers ("strength(s) of the constraint potential(s)"), $w^i(\vec{r})$ is an atom-centered weight function, and N_c is the target value of the constraint. Multiple constraints can be included in a CDFT simulation by use of the sum over c. The weight function is constructed as a normalized sum over selected constraint atoms $\mathcal{C}$

$$w^i(\vec{r}) = \frac{\sum_{j \in \mathcal{C}} c_j P_j(\vec{r})}{\sum_{j \in \mathcal{N}} P_j(\vec{r})} \tag{2.11}$$

where c_j are atomic coefficients which determine how each atom is included in constraint, P_j is the so-called cell function which determines the volume occupied by atom j according to some population analysis method, and $\mathcal{N}$ is the set of all atoms in a system. The Becke [16] and Hirshfeld [17] space partitioning schemes can be used as constraint weight functions in CP2K. The CDFT energy expression, E_{CDFT}, is solved self-consistently using a two-tiered approach: one external optimization loop for constraints, and an inner loop to converge the electronic structure. By definition,

all constraints are satisfied when

$$\vec{c}_{\vec{\lambda}} = \left[\sum_{i=\uparrow,\downarrow} \int w_1^i(\vec{r}) n^i(\vec{r}) d\vec{r} - N_1, ... \right]^T = \vec{0} \tag{2.12}$$

The constraint Lagrangian multipliers $\vec{\lambda}$ can therefore be optimized by minimizing the constraint error expression $\max|\vec{c}_{\vec{\lambda}}|$ until the largest element decreases below a threshold ϵ. Root-finding algorithms are used to optimize $\vec{\lambda}$.

2.5 Preparation of surfaces and geometry minimization

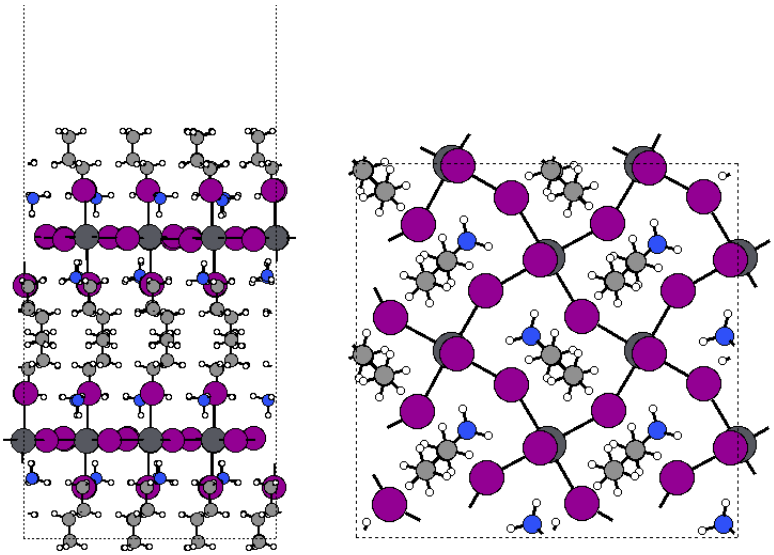

Figure 2.1: Relaxed BA_2PbI_4 (001) surface. Left figure shows side view (the vacuum at the top of the unit cell is cut for clarity). Right figure shows top view. (Colors: dark gray - Pb, purple - I, light gray - C, blue - N, white - H)

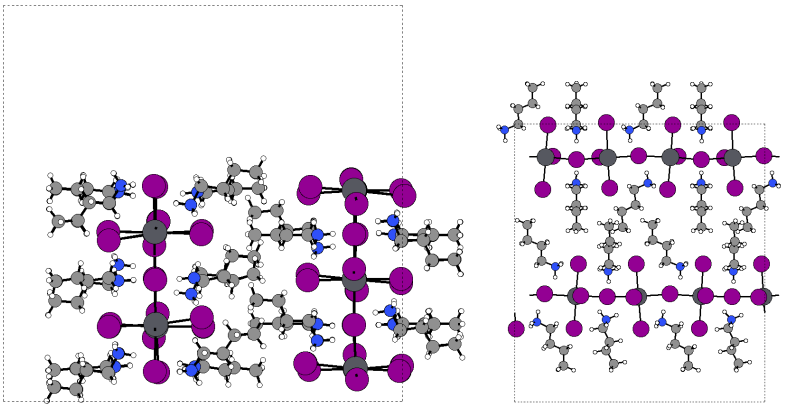

Figure 2.2: Relaxed BA_2PbI_4 (110) surface. Left figure shows side view. Right figure shows top view. (Colors: dark gray - Pb, purple - I, light gray - C, blue - N, white - H)

To obtain the structures that can be used as initial structures in geometry optimisation calculations, we constructed surfaces from bulk structures of appropriate perovskites. This was done using the python module *Atomic Simulation Environment* (ASE) [18] and the *QuantumATK* modeling software [19]. The surface with (001) Miller indices was obtained by separating two layers of $n = 1$ perovskites between organic molecular cations. Computational cell with these two layers was than extended in the $\hat{z}$ direction by at least 10 Å of vacuum to ensure no interaction between periodic images of opposing surfaces. Care had to be taken to obtain neutral surfaces with preserved organic molecular cations. Afterwards, the cells were replicated in $\hat{x}$ and $\hat{y}$ directions to obtain bigger cells to prevent oxygen from interacting with its periodic images, as we wish to isolate the sole effects of oxygen adsorption to the surface. Figure 2.1 shows the cell of the relaxed BA_2PbI_4 (001) surface when viewed from the side or from the top. A similar procedure was carried out for the surface with (110) Miller indices.

Figure 2.2 shows the relaxed BA_2PbI_4 (001) surface when viewed from the side or from the top. Table 2.1 shows details for these two pristine surfaces. ASE was also used to add an oxygen molecule to the surfaces as it offers easy tools for translation and rotation of parts of the structures, enabling a simple preparation of initial structures.

Perovskite	surface	a, b, c (Å)	supercell type	n_{atoms}	formula
BA_2PbI_4	(001)	17.753, 17.385, 57.601	2x2x2	624	16(BA_2PbI_4)
BA_2PbI_4	(110)	24.848, 27.601, 27.421	2x1x2	780	20(BA_2PbI_4)

Table 2.1: Details of initial structures for (001) and (110) surfaces of BA_2PbI_4.

The main calculations carried out in this work are geometry optimizations of perovskite surfaces with or without adsorbed oxygen. Geometry optimization is carried out using *Broyden–Fletcher–Goldfarb–Shanno* (BFGS) algorithm [20] where atoms are moved inside the unit cell in a way to minimise the force on each of them. Each step of geometry optimisation involves self-consistent solution of the Kohn-Sham equation to find energies and densities.

2.6 Choice of the functional and PW cutoff convergence

The functional used is 'vdW-DF-cx' which stands for *van der Waals density functional with consistent exchange* [21]. This functional includes van der Waals forces from first principles, and the exchange correlation functional depends only on the density and its gradients in a nonlocal manner. When considering adsorption of molecules to surfaces it is important to include all relevant contributions such as van der Waals forces, with van der Waals forces being responsible for physical adsorption (physisorption) [22].

In order to find a satisfactory balance between accuracy and efficiency and avoid convergence issues, the plane-wave (PW) cutoff convergence was analysed. This was done using an experimental structure of PbI_2 (cell parameters and atoms positions obtained experimentally) [23]. The procedure involves calculating the energy for different cutoff parameters with the expectation of that the energy should converge, as increasing the cutoff increases the accuracy of the calculation. Using an experimental structure is a simpler strategy then using structures relaxed via geometry optimisation with some particular cutoff value which will always show bias towards that value of the cutoff.

Table 2.2 shows the evolution of the energy relative to the minimum with the change of the cutoff. Also shown is the number of Gaussians on each grid of CP2K's multi-grid levels. The distribution of points should be balanced covering all grids; if finer grids (higher number grids) are not populated, accuracy will be negatively affected. In the table the coarsest grid is not populated for higher values of cutoff, which leads to a decrease of efficiency. The minimum of energy is achieved for 520 Ry which is also the point on which Gaussians are distributed equally. The same analysis method was also performed with biased structures similar to the ones used in our main calculations (BA_2PbI_4 bulk and (001) surface structures), which show balanced distribution of grid points around 720 Ry. This value was chosen as a compromise between accuracy and efficiency. The procedure was also repeated for vdW cutoff parameter with PW cutoff set at 720 Ry, which corresponds to the cutoff of the fast Fourier transform grid used in the calculation of the nonlocal vdW functional. Figure 2.3 shows the dependence of the energy on the vdW cutoff parameter (chosen to be 50 Ry). The values of all other parameters can be seen in appendix A which shows an example CP2K input file.

PW cutoff (Ry)	E-E_{min} (10^{-6}Ha)	Grid 1	Grid 2	Grid 3	Grid 4
420	1.686	14351	119090	57283	20900
520	0	10249	110336	44615	46424
620	1.544	2049	84692	78203	46680
720	0.777	0	61983	92487	57154
820	1.215	0	57875	85980	67769
920	1.685	0	55807	88048	67769
1020	1.506	0	47569	87950	76105
1120	1.407	0	26677	108842	76105
1220	1.311	0	18453	114988	78183

Table 2.2: Energy differences to minimum value and multi-grid distribution of Gaussians for different values of cutoff parameter. Calculated using the experimental structure of PbI_2.

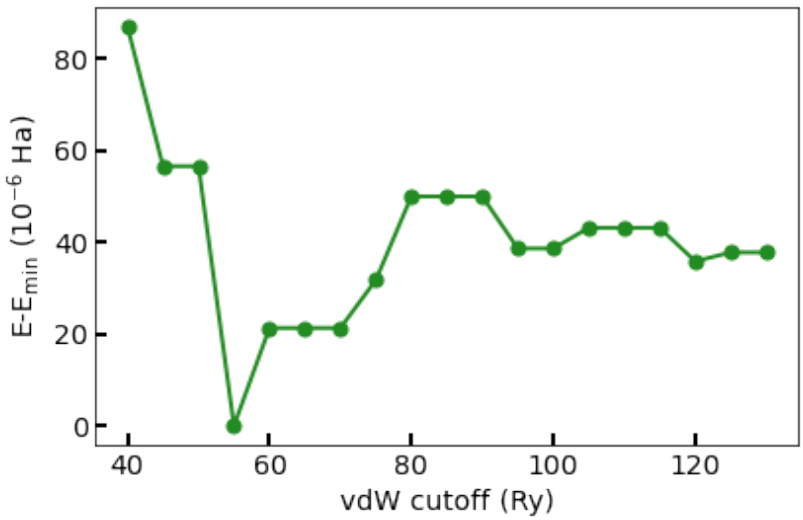

Figure 2.3: Dependence of energy relative to minimum on vdW cutoff value. Calculated using the experimental structure of PbI_2 with PW cutoff of 720 Ry.

3 Results and discussion

In the context of the degradation of quasi-2D perovskites, we focus our investigation on the interaction of 2D perovskite surfaces with molecular oxygen. To this end, in a set of preliminary calculations, the binding energies of adsorption of oxygen to BA_2PbI_4 (001) and (110) surfaces were calculated. Afterwards, a scan of initial position of oxygen on the surfaces was performed to get dependence of binding energy on the z coordinate for the (001) surface and on (x, y) coordinates for the (110) surface. Finally, the electron transfer energies were calculated using CDFT to investigate the likelihood of degradation through the formation of a reactive superoxide ion O_2^-. The binding energy E_b is defined as:

$$E_b = E_{\text{system}} - (E_{\text{surface}} + E_{\text{adsorbate}}) \tag{3.1}$$

in our case, "system" is the surface including oxygen, "surface" is the (001) or (110) surface and the adsorbate is an oxygen molecule. In the above, each energy component is intended to be defined for the corresponding relaxed geometry. This most likely corresponds to a local minimum when treating the combined "system". The definition of adsorption energy E_a differs from binding energy definition only by sign. The electron transfer energy E_{ET} is defined as

$$E_{\text{ET}} = E_{\text{CDFT}} - E_{\text{DFT}} \tag{3.2}$$

where E_{CDFT} is the energy of the charge separated system obtained using CDFT and E_{DFT} is the energy obtained using regular DFT without any constraints on charges. In this case, the electron transfer is assumed to occurred at frozen geometry, i.e. we do not perform any geometry relaxation within CDFT calculations.

3.1 Preliminary calculations

In the first round of calculations, a geometry optimisation was carried out for surfaces prepared as previously discussed. The oxygen molecule was also relaxed using a large computational box filed with vacuum. The size of the computational box needs to be sufficiently large to avoid the oxygen molecule interacting with its periodic images.

The spin state of oxygen was set to triplet, as it is the ground state of neutral oxygen. Initial geometry optimisation of a O2 molecule in vacuum was performed using a computational cell with side lengths of 10 Å and value of PW cutoff parameter of 360 Ry. This calculation had convergence problems so the box size was increased to 25 Å, and the PW cutoff was increased to 720 Ry after cutoff convergence analysis. This resolved convergence problems. The calculated neutral oxygen bond length is 1.230 Å which is slightly longer than experimental value of 1.208 Å [24]. With these calculations, the reference energies for BA_2PbI_4 (001) surface, BA_2PbI_4 (110) surface and oxygen molecule were obtained.

Surface	#	E_b (eV)	c.-c. distance (Å)	O_2 z_{cm} (Å)	location
(001)	1	-0.070	2.285	30.839	above BA
(001)	2	-0.081	2.375	30.836	above BA
(001)	3	-0.196	2.235	27.640	above I
(001)	4	-0.194	1.925	27.451	above I
(110)	5	-0.089	3.185	18.074	above I
(110)	6	-0.077	3.935	18.157	above I
(110)	7	-0.119	3.025	16.976	above BA

Table 3.1: Preliminary calculations results for BA_2PbI_4.

Using the final relaxed geometries, the oxygen molecule was added to the surfaces using ASE to obtain initial structures that will be used to obtain adsorption energies for various interesting initial positions of the oxygen molecule. While relaxing the isolated oxygen molecule or a surface with oxygen, the spin state was set to triplet as it is the ground state of a oxygen molecule. Here, in these preliminary calculations, few different initial positions of the oxygen on the surface were chosen to get an idea of the values of binding energies. We explored the interesting parts of the surfaces where a systematic scan of initial positions of oxygen could be performed. After performing geometric relaxation of the BA_2PbI_4 (001) surface, it was found that the strongest adsorption between oxygen and the surface is achieved with the oxygen placed in the cavity above an iodine atom, between organic cations. This can be seen in the Table 3.1 where calculations 1 and 2 are the above organic cation and calculations 3 and 4 are above an iodine atom. Closest-contact distances are similar, yet different positions on the surface strongly affect the obtained energy values. The closest-contact distance is calculated as the distance to the first peak in the radial distribution function with oxygen as the reference point. For the BA_2PbI_4

(110) surface it was found that the adsorption energy depended strongly on the initial position of oxygen relative to the surface, both on distance to the surface as well as the (x, y) location on the surface. This is a consequence of the presence of cavities and several distinct atomic groups on this surface. This can be seen in the Table 3.1 where calculations 5 and 6 are conducted for oxygen above different iodine atoms and calculation 7 is conducted for oxygen above an organic BA molecule.

3.2 Surface scan of O_2 initial positions

3.2.1 BA_2PbI_4 (001) surface z axis scan

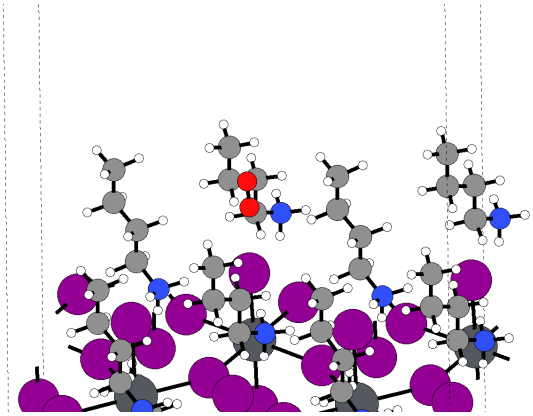

Figure 3.1: Initial position of oxygen inside molecular cavity above iodine atom for (001) surface. Figure shows tilted view with only uppermost atoms. (Colors: dark gray - Pb, purple - I, light gray - C, blue - N, white - H, red - O)

After the initial calculations of BA_2PbI_4 (001) surface with oxygen, we decided to investigate binding energy values in a systematic fashion by performing a scan along the direction perpendicular to the surface, with the oxygen was placed in the molecular cavity above an iodine atom, see Figure 3.1. The scan was performed by taking multiple equidistant initial positions for oxygen, constraining only the z coordinate at a different value for each step of the scan. Practically, from each initial O_2 position geometry optimisation was performed with a fixed z coordinate of one oxygen atom and also several iodine atoms from the opposite side of the surface, to prevent the entire surface drifting away from oxygen. From this scan we can obtain insight into the sensitivity of the binding energy to the distance of the O_2 to the surface, i.e. we can construct a potential energy surface in respect to the constrained coordinate z.

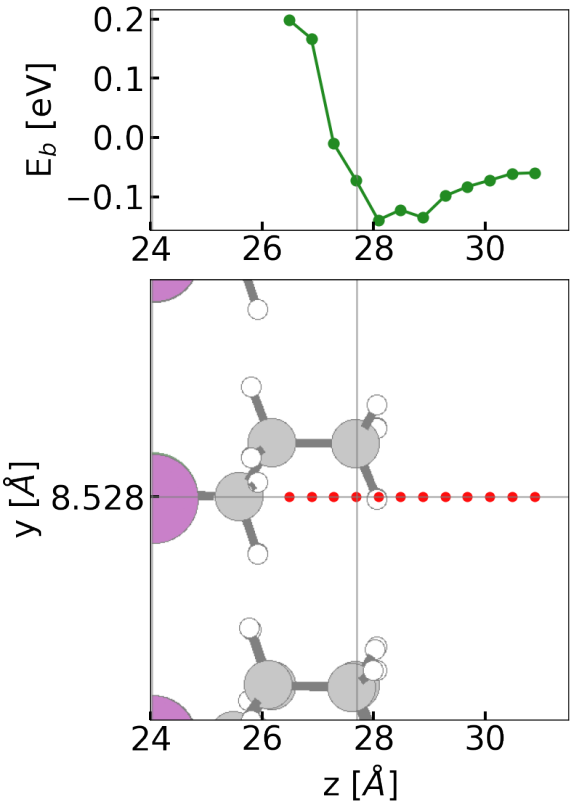

Figure 3.2: Top frame shows BA_2PbI_4 (001) surface binding energy in dependence on the z coordinate of oxygen molecule. The bottom frame shows initial positions of oxygen center of mass relative to the surface. (Colors: purple - I, light gray - C, white - H)

The top frame of Figure 3.2 shows how the energy changes with the initial position of the oxygen molecule. The bottom frame of Figure 3.2 shows the initial oxygen positions relative to the surface. The surface is shown from a side view and the oxygen is not overlapping with other atoms. Minima are obtained for a distance of 4-5 Å between oxygen and iodine. Adsorption at these distances and with these energy values corresponds to physisorption, which is characterized by low binding energies of 10-100 meV and by relatively large equilibrium separation of 3-10 Å [25]. As oxygen gets closer to iodine, it is repelled and does not form any strong chemical bonds with iodine. The behaviour for positions far from the surface and moving away from the surface should be asymptotically approaching 0 in an ideally infinite-size box.

We can compare our value of minimum of binding energy for (001) surface of BA_2PbI_4 with same quantity for $MAPbI_3$ of -0.28 eV which was calculated for oxygen adsorbing to hollow site between two MA^+ cations [26], this value was calculated on a 1x1 slab cell with similar computational details and with similar functional used. Our value for minimum of binding energy of -0.14 eV shows weaker adsorption in

comparison and indicates better stability to oxygen for BA_2PbI_4.

This result is an expected behavior for molecular oxygen not chemically interacting with the surface. Such O_2 physisorption does not directly translate into a surface degradation, however it could have important implications for the device efficiency and therefore relevant for applications. Besides, a stable presence of oxygen at these distances could be a step towards photo-induced degradation. Oxygen first weakly adsorbs to surface and after the perovskite is photo-excited a transfer of one electron from the surface could take place, forming the more reactive superoxide.

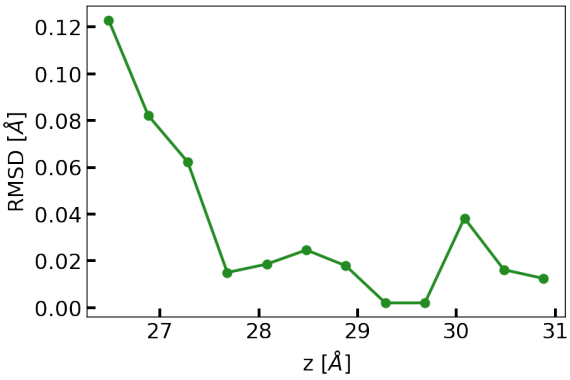

Figure 3.3: Root-mean square deviation (RMSD) of atoms positions for (001) surface.

Figure 3.3 shows the root-mean square deviation (RMSD) of atoms position for (001) surface for same set of points of oxygen as Figure 3.2. This value show how far atoms globally move from their equilibrium (i.e. non-interacting) positions. As would be expected, this value is highest for the oxygen position closest to the surface, producing a similar profile to the binding energy. Generally, the magnitude of these RMSD values are small, indicating that there is not too much disturbance of atomic positions by addition of oxygen - in line with physisorption phenomenology.

3.2.2 BA_2PbI_4 (110) surface x-y plane scan

The BA_2PbI_4 (110) surface shows a lot of variety in its surface atoms which suggests that an in-plane scan parallel to surface is the optimal choice. We therefore decided to perform a scan on a grid of points spanned by 4 points in the x direction and 5 points in the y direction. Figure 3.4 (left) shows the top view of the surface with marked initial positions of oxygen in red. Each initial point was then used to perform a geometry optimisation calculation with constrained x and y coordinates of one of the oxygen atoms. In order to get comparable values, initial z coordinates had to

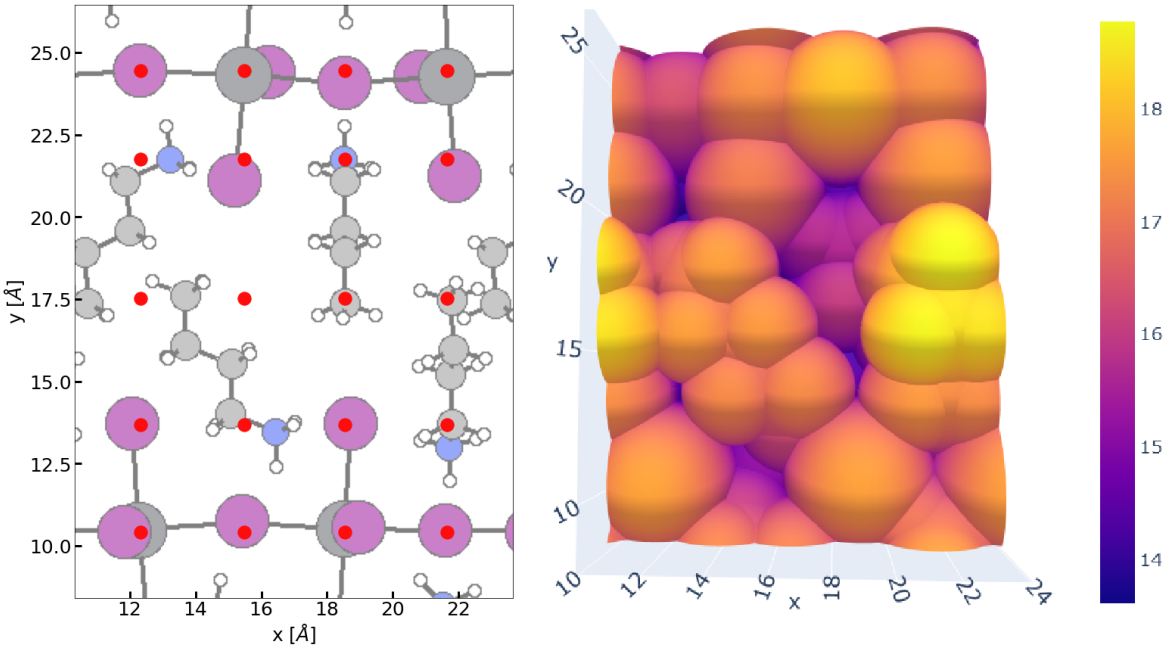

Figure 3.4: Left figure shows top view of BA_2PbI_4 (110) surface with marked initial positions of oxygen (in red). (Colors: dark gray - Pb, purple - I, light gray - C, blue - N, white - H) Right figure shows top view of extended van der Waals BA_2PbI_4 (110) surface with colors indicating z coordinate in Å.

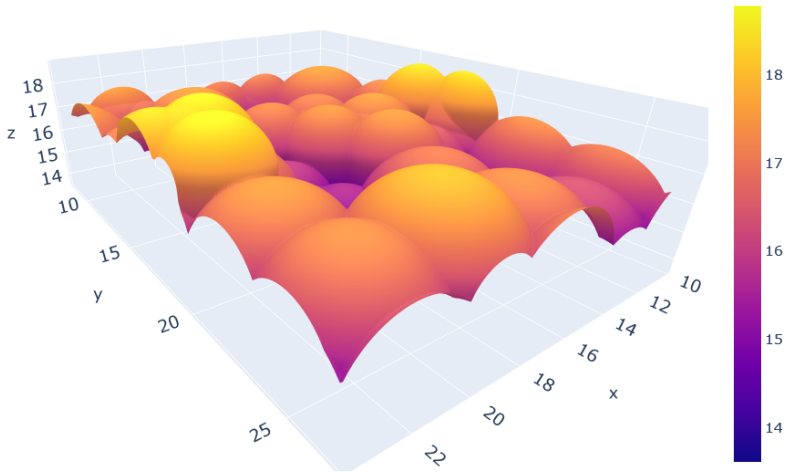

Figure 3.5: Side view of extended van der Waals surface.

be chosen so that oxygen is homogeneously displaced from the surface. To achieve this, oxygen was placed on top of the extended van der Waals surface, which was generated by drawing spheres around each surface atom i with radii $r_i^{eVdW} = r_i^{VdW} + \frac{1}{2}r_O^{VdW}$. Figure 3.4 (right) shows the top view of extended van der Waals surface,

while Figure 3.5 also illustrates this extended van der Waals surface. This was done in python with the help of the ASE module.

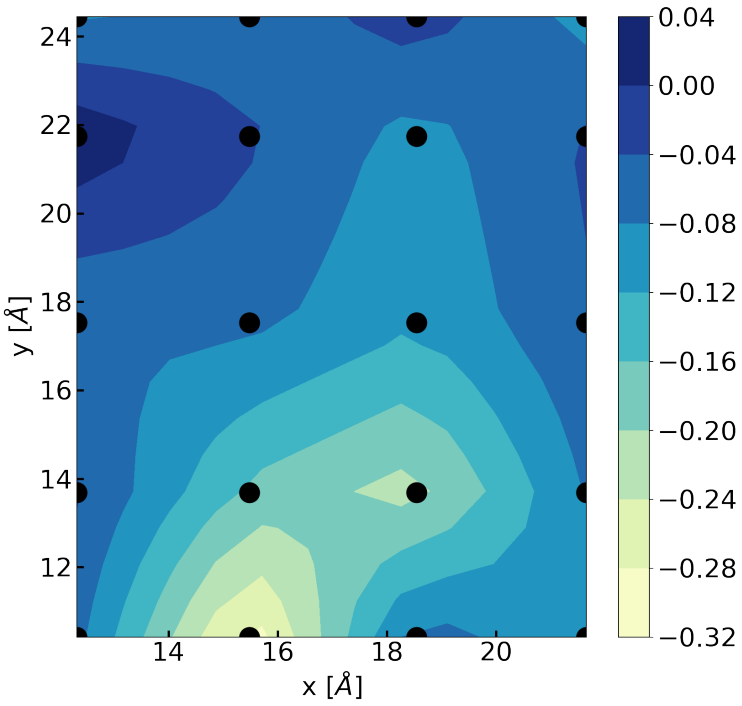

Figure 3.6: Heat map of the binding energy of oxygen in eV for the BA_2PbI_4 (110) surface.

The results can be seen on Figure 3.6 in the form of a heat map with values in between calculated points being linearly interpolated. The obtained values of the binding energy range from around -0.3 eV to 0.001 eV. The strongest adsorption is obtained when the oxygen is placed in a cavity surrounded by iodine ions while the weakest adsorption is obtained if oxygen is placed in the organic cavity above nitrogen. Interestingly, several of such sampled points fall above iodine atoms, but the largest binding energy is for the bridging I connecting two octahedra, forming an actual cavity with in-plane close contacts with other 2 iodine atoms. In most other cases oxygen is weakly adsorbed to the surface through physisorption.

Figure 3.7 shows distance to closest-contact of oxygen. Closest-contact distances ranging from 1.8 Å to 3 Å are mostly consistent with physisorption, however points where this distance is smaller also show stronger adsorption in binding energy. These points could be considered possible chemisorption sites. Chemisorption of oxygen to these sites could be an important effect of degradation of 2D perovskites and should

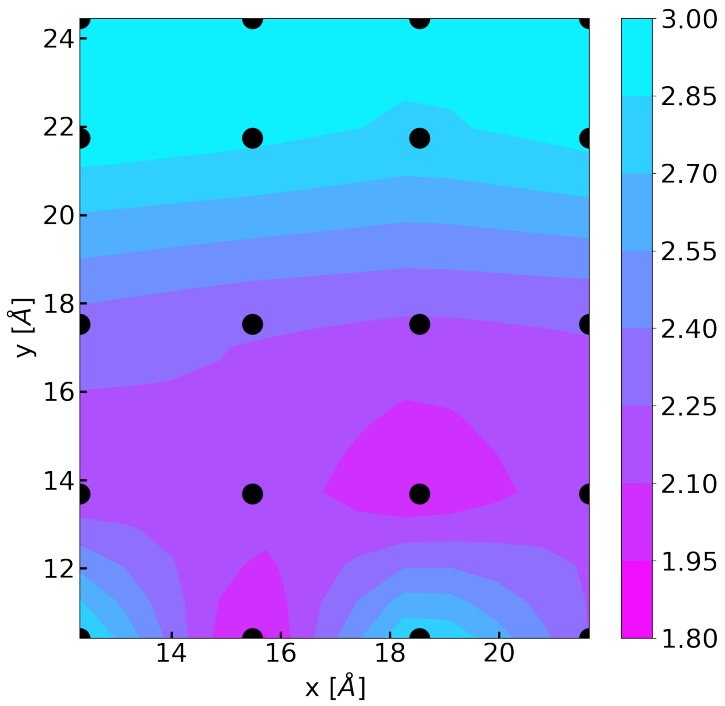

Figure 3.7: Heat map showing distance to the closest-contact of oxygen after geometry optimisation in Å.

be investigated further by doing z coordinate scans of the binding energy. Overall, oxygen is adsorbed to several possible sites on (110) surface, which could lead to lower efficiencies and possible degradation by additional effects.

3.3 Electron transfer energies

Using final geometry configurations from previous calculations we can calculate electron transfer energies. Figure 3.8 shows electron transfer energies calculated for final points of the BA_2PbI_4 (001) surface scan. As oxygen is moving away from the surface, the barrier for electron transfer is increasing until it reaches a certain point and changes become smaller. These energies are between 4.2 eV and 5.8 eV which falls at the edge of solar spectrum. With such energy ranges, it is not unrealistic to consider electron transfer processes happening after light excitation. However excitons in 2D perovskites absorb at lower energies and hence we should exclude the formation of highly-reactive superoxide ions, that determine the photooxidation of quasi-2D perovskite.

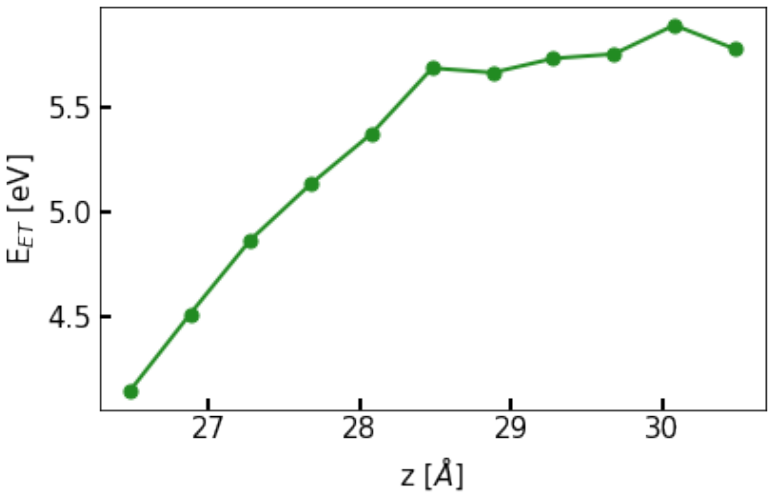

Figure 3.8: Electron transfer energy dependence on the oxygen z coordinate for BA_2PbI_4 (001) surface.

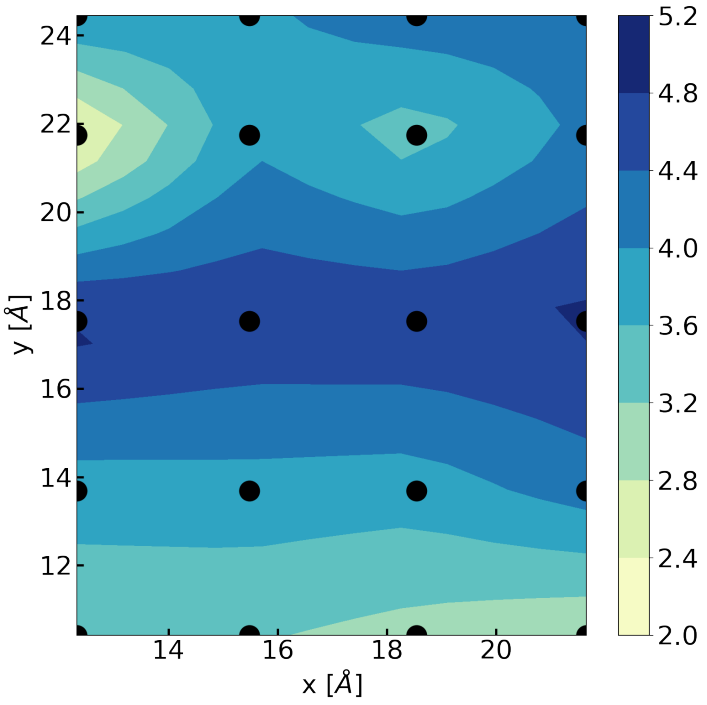

Figure 3.9: Heat map of electron transfer energies in eV for BA_2PbI_4 (110) surface.

Figure 3.9 shows a heat map of electron transfer energies calculated from final configurations of BA_2PbI_4 (110) surface xy plane scan calculations. Smaller values of electron transfer energies are obtained for oxygen above inorganic sites. This is a consequence of screening. The minimum value is for oxygen placed in a cavity above nitrogen which is explained by nitrogen having positive charge that neutralizes

the negative charge on oxygen. Here, values range from around 2.5 eV to 5 eV, where several values fall into solar spectrum energies and with comparable energies to excitons in 2D perovskites, amounting to around 2-3 eV [27]. This result more clearly indicates this surface-oxygen interaction scheme as potentially compatible with degradation mechanism through photooxidation and generation of a superoxide ion. Every plot in the results section was drawn using python module *matplotlib* [28] and every figure of structures was created using ASE.

4 Summary and outlook

4.1 Summary

Calculations of adsorption energies of oxygen on BA_2PbI_4 (001) and BA_2PbI_4 (110) surfaces were performed using CP2K computational software based on Gaussian and plane wave approach to DFT. To calculate binding energies, a z axis scan of initial positions of oxygen on the BA_2PbI_4 (001) surface was performed. The results show weak adsorption of oxygen to surfaces with adsorption energies around 0.1 eV, with the binding energy minimum being at oxygen-iodine distances of around 4-5 Å. This type of adsorption is described as physisorption. Binding energy calculated with xy plane scan of BA_2PbI_4 (110) surface similarly show physisorption tendencies, but having some stronger adsorption points with adsorption energies of 0.3 eV, which should be further investigated. Electron transfer energies calculated using constrained DFT are consistent with possible degradation by photooxidation of perovskite and generation of superoxide.

4.2 Outlook

The applied method of calculating binding energies and electron transfer energies could also be used to study many other perovskites. In order to get a better insight into degradation of quasi-2D perovskites it is necessary to study different degradation mechanisms. Sensitivity to moisture could also be studied by looking at adsorption of water. Effects of vacancies or other impurities of the surface could be studied using similar approach with geometry relaxation of the surface.

Appendices

Appendix A Example of CP2K input file

```
&GLOBAL
  PRINT_LEVEL LOW
  WALLTIME 180500
  PROJECT BAIO2
  RUN_TYPE GEOMETRY_OPTIMIZATION
&END GLOBAL

&MOTION
  #Geometry optimization parameters
  &GEO_OPT
    OPTIMIZER BFGS
    MAX_ITER 1000
  &END GEO_OPT

  #Constraint of listed atoms z coordinate
  &CONSTRAINT
    &FIXED_ATOMS
      COMPONENTS_TO_FIX Z
      LIST 1 85 89 93 94 95 96 97 98
    &END FIXED_ATOMS
  &END CONSTRAINT
&END MOTION

&FORCE_EVAL
  METHOD QUICKSTEP
  &DFT
    #Charge and spin state
    CHARGE 0
    MULTIPLICITY 3

    #Spin polarized calculation
    LSD

    #Basis set and pseudopotential files
    BASIS_SET_FILE_NAME ../filesforcp2k/BASIS_MOLOPT_UCL
```

```
    BASIS_SET_FILE_NAME ../filesforcp2k/BASIS_MOLOPT
    POTENTIAL_FILE_NAME ../filesforcp2k/GTH_POTENTIALS

    #Specification of cutoff parameters
    &MGRID
      CUTOFF 720
      REL_CUTOFF 60
    &END MGRID

    #Energy minimization parameters
    &SCF
      SCF_GUESS RANDOM
      EPS_SCF 5.e-7
      MAX_SCF 50
      &OT
        MINIMIZER DIIS
        N_DIIS 7
        PRECONDITIONER FULL_KINETIC
      &END OT
      &OUTER_SCF
        TYPE NONE
        OPTIMIZER NONE
        EPS_SCF 5.0E-7
        MAX_SCF 25
      &END OUTER_SCF
    &END SCF

    #Specification of functional
    &XC
      &XC_FUNCTIONAL
        &GGA_X_LV_RPW86
        &END GGA_X_LV_RPW86
        &PW92
        &END PW92
      &END XC_FUNCTIONAL
      &vdW_POTENTIAL
         DISPERSION_FUNCTIONAL NON_LOCAL
         &NON_LOCAL
            TYPE DRSLL
            VERBOSE_OUTPUT
```

```
            KERNEL_FILE_NAME ../filesforcp2k/vdW_kernel_table.dat
            CUTOFF 50
          &END NON_LOCAL
        &END vdW_POTENTIAL
      &END XC
    &END DFT

    &SUBSYS
      #Cell parameters
      &CELL
A     17.7527999434        0.0000000000        0.0000000000
B      0.0000000000       17.3849999445        0.0000000000
C      0.0000000000        0.0000000000       57.6013999121
      &END CELL

      #.xyz file containing initial structure
      &TOPOLOGY
        COORD_FILE_FORMAT XYZ
        COORD_FILE_NAME ./structure.xyz
        CONNECTIVITY OFF
      &END TOPOLOGY

      #Choice of basis set and pseudopotential for each element used
      &KIND H
        BASIS_SET TZV2P-MOLOPT-GTH
        POTENTIAL GTH-PBE-q1
      &END KIND
      &KIND I
        BASIS_SET TZV2P-MOLOPT-SR-GTH
        POTENTIAL GTH-PBE-q7
      &END KIND
      &KIND C
        BASIS_SET TZV2P-MOLOPT-GTH
        POTENTIAL GTH-PBE-q4
      &END KIND
      &KIND N
        BASIS_SET TZV2P-MOLOPT-GTH
        POTENTIAL GTH-PBE-q5
      &END KIND
      &KIND Pb
```

```
      BASIS_SET TZV2P-MOLOPT-SR-GTH
      POTENTIAL GTH-PBE-q4
    &END KIND
    &KIND O
      BASIS_SET TZV2P-MOLOPT-GTH
      POTENTIAL GTH-PBE-q6
    &END KIND
  &END SUBSYS

  #Printing of forces
  &PRINT
    &FORCES
    &END FORCES
  &END PRINT
&END FORCE_EVAL
```

5 Prošireni sažetak

5.1 Uvod

Hibridni anorgansko-organski halogenidni perovskiti su obećavajuća klasa materijala za primjenu u optoelektroničkim uređajima kao što su solarne ćelije, diode i laseri. Perovskiti dijele slična strukturalna svojstva s istoimenim mineralom $CaTiO_3$. Mnoštvo zanimljivih svojstava dolazi od njihove mekane rešetke i dinamički uneređene kristalne strukture koja pozitivno mijenja njihova vremena rekombinacije nositelja naboja.

2D perovskiti dobiveni kemijskim smanjenjem dimenzionalnosti 3D kristalne rešetke predstavljaju proširenje u sastavnoj raznolikosti perovskita te omogućavaju širu prilagodbu svojstava perovskita. Jedna od prepreka prije šire upotrebe perovskita je pitanje njihove stabilnosti. Općenito je primijećeno da vanjski uvjeti kao što su vlaga, povišene temperature, kisik i ultra-ljubičasto zračenje uzrokuju nestabilnost uređaja češće nego kod uobičajenih fotonaponskih materijala. Posebice je pokazano da izlaganje fotoaktivnih slojeva $CH_3NH_3PbI_3$ svjetlosti i kisiku vodi do nastanka vrlo reaktivnog (O_2^-) superoksida te daljnje kemijske degradacije.

U ovome radu su primijenjene računalne metode bazirane na teoriji funkcionala gustoće za proučavanje adsorpcije kisika na površine kvazi-2D perovskita butil olovo jodida BA_2PbI_4. Također je razmatran prijelaz elektrona s površine na kisik koji opisuje degradaciju preko reaktivnog superoksida.

5.2 Metoda

Teorija funkcionala gustoće (engl. DFT) bazirana je na dva rada Kohn-a u kojima se predstavlja teorijska pozadina te upute za provedbu DFT izračuna. Glavna ideja je u tome da vanjski potencijal U u kojem se čestice gibaju ovisi jedino o gustoći čestica $n(\vec{r})$ u osnovnom stanju. Također energija sustava $E[n]$ je funkcional gustoće čestica $n(\vec{r})$, dok je energija osnovnog stanja globalni minimum ovog funkcionala i gustoća čestica ovog globalnog minimuma je osnovno stanje gustoće čestica. Točna gustoća čestica sustava $n(\vec{r})$ može se prikazati kao gustoća čestica pomoćnog sustava (Kohn-Sham sustava) ne-međudjelujućih čestica. Svaka Kohn-Sham čestica se giba u ne lokalnom Kohn-Sham potencijalu, V_{KS}, koji ima nekoliko doprinosa: U vanjski

potencijal, V_H Hartree potencijal (Coulombov potencijal ostalih čestica) i potencijal izmjene i korelacije V_{xc}. Uzimajući sve ovo u obzir dobivamo Schrödingerovu jednadžbu za Kohn-Sham čestice:

$$\left[-\frac{\hbar^2}{2m}\vec{\nabla}^2 + U(\vec{r}) + V_H(\vec{r})\right]\psi_m(\vec{r}) + \int d\vec{r'}V_{xc}(\vec{r'},\vec{r})\psi_m(\vec{r'}) = e_m\psi_m(\vec{r}) \tag{5.1}$$

što je trodimenzionalna parcijalna diferencijalna jednadžba. Gustoća Kohn-Sham čestica u osnovnom stanju može se izračunati iz valnih funkcija:

$$n(\vec{r}) = \sum_{\text{popunjena stanja}} |\psi_n(\vec{r})|^2 \tag{5.2}$$

Kohn-Shamov potencijal ovisi o gustoći čestica stoga potencijal, gustoće i valne funkcije trebaju biti izračunate samosuglasno.

Za DFT izračune koristio se CP2K programski paket otvorenog koda za izračun elektronske strukture i molekularne dinamike. Pristup DFT-a korišten u CP2K-u je pristup baziran na Gaussianima i ravnim valovima (engl. GPW). U ovome pristupe se za razvoj orbitalnih funkcija koristi kontrahirana baza Gaussiana $g(\vec{r})$:

$$\phi\left(\vec{r}\right) = \sum_u d_u g_u\left(\vec{r}\right) \tag{5.3}$$

gdje su kontrahirani koeficijenti d_u fiksni, a primitivni Gaussiani

$$g\left(\vec{r}\right) = r^l \exp\left[-\alpha\left(\vec{r}-\vec{A}\right)^2\right] Y_{lm}\left(\vec{r}-\vec{A}\right) \tag{5.4}$$

su centrirani na pozicijama atoma. Ove funkcije su definirane s eksponentom α, kuglinim funkcijama Y_{lm} s kutnim momentom (l, m) i koordinatama središta atoma $\vec{A}$. CP2K koristi razna svojstva Gaussiana za efikasno i precizno rješavanje problema. U ovome pristupu se također koristi razvoj periodičnih funkcija (kao što je gustoća čestica) po ravnim valovima.

Korišteni funkcional je 'vdW-DF-cx', van der Waals funkcional gustoće s konzistentnom izmjenom. Ovaj funkcional sadrži van der Waalsove sile uključene iz prvih principa. Kako se u ovome radu razmatra adsorpcija molekula na površine van der Waalsovo međudjelovanje je neizostavan doprinos koji i opisuje fizikalnu adsorpciju (fizisorpciju).

U ovome radu jedan od glavnih izračuna su bile geometrijske optimizacije površina perovskita s ili bez adsorbiranog kisika. Geometrijska optimizacija se sastoji od provođenja *Broyden–Fletcher–Goldfarb–Shanno* (BFGS) algoritma koji pomiče atome unutar ćelije tako da minimizira sile na atoma. U svakome koraku geometrijske optimizacije se provodi minimizacija energije unutar DFT-a. Nakon provedbe geometrijske optimizacije provodi se izračun s ograničenom teorijom funkcionala gustoće (engl. CDFT) kako bi se izračunala energija prijenosa elektrona. CDFT omogućava provedbu lokalizacije naboja na kisik tako da se u izrazu za energiju dodaju potencijali centrirani na atomima koji nakon minimizacije osiguravaju lokalizaciju naboja.

Početne strukture površina dobivene su isijecanjem iz njihovih volumnih struktura koristeći računalne alate *Atomistic Simulation Environment* (ASE) i *QuantumATK*. Površine su postavljene u računalne ćelije tako da su duž x, y ravnine, a u z smjeru imaju barem 10 Å vakuuma.

5.3 Rezultati

Za početak su izračunate energije površina i molekule kisika koristeći geometrijsku optimizaciju. Za molekulu kisika je korištena ćelija sa stranicama duljine 25 Å s kisikom u sredini. Ovime su dobivene referentne energije potrebne za izračun energije vezanja E_b koja je definirana kao:

$$E_b = E_{\text{sustav}} - (E_{\text{površina}} + E_{\text{adsorbat}}) \tag{5.5}$$

Nakon izračuna s kisikom pri kojima je bilo problema s konvergencijom napravljena je analiza cutoff parametra. Za eksperimentalnu strukturu PbI_2 minimizirana je energija za različite vrijednosti cutoff parametra. Rezultati su prikazani u tablici 2.2. Za cutoff parametar je odabrana vrijednost od 720 Ry koja je razriješila problem konvergencije kod kisika te ima zadovoljavajuću preciznost. Sljedeće je dodan kisik na zadnje konfiguracije geometrijski optimiziranih površina. Molekula kisika i površine koje su sadržavale kisik pri izračunima su bile u stanju tripleta koje je osnovno stanje kisika. U početnim izračunima pozicija kisika na površini je bila proizvoljna, istražujući zanimljive pozicije na površinama gdje bi se mogao provesti sistematski izračun ovisnosti energija vezanja. Za (001) površinu je napravljen pregled ovisnosti energije vezanja o z koordinati kisika. Kisik s fiksiranom z koordinatom je postavljen iznad

atoma joda u šupljini molekularnih kationa. Slika 3.2 pokazuje dobivenu ovisnost i položaj kisika u odnosu na površinu. Minimum energije vezanja je dobiven za 4-5 Å udaljenosti kisika i joda. Energija minimuma od oko -0.14 eV odgovara fizisorpciji. Ova vrijednost je uspoređena s vrijednošću za adsorpciju na $MAPbI_3$ od -0.28 eV dobivenu sličnom metodom. Ovo pokazuje da BA_2PbI_4 slabije adsorbira kisik i stabilniji je od $MAPbI_3$.

Za (110) površinu je napravljen pregled ovisnosti energija vezanja o x, y koordinati kisika. Kisik je postavljen na proširenu van der Waalsovu površinu (proširena za pola vdW radijusa kisika) s fiksiranim x i y koordinatama jednog njegovog atoma. Slika 3.4 (lijevo) pokazuje pozicije kisika u odnosu na površinu, a (desno) je prikazana proširena van der Waals površina kao i na slici 3.5 iz drugog pogleda. Slika 3.6 pokazuje kartu topline energija vezanja. Dobivene vrijednosti energija vezanja su između -0.3 eV i 0.001 eV što pokazuje uglavnom slabo vezanje odnosno fizisorpciju. Na nekoliko mjesta je dobiveno jače vezanje što su moguća kemisorpcijska mjesta koja bi mogla biti odgovorna za degradaciju.

Koristeći konačne konfiguracije prethodnih izračuna s CDFT-om izračunate su energije sustava u kojima je jedan dodatni elektron lokaliziran na molekuli kisika. S ovime su izračunate energije prijenosa elektrona E_{ET} prema formuli:

$$E_{ET} = E_{CDFT} - E_{DFT} \tag{5.6}$$

Za (001) površinu dobivene vrijednosti su prikazane na slici 3.9. Dobivene vrijednosti su između 4.2 eV i 5.8 eV što pripada rubu sunčevog spektra. Ovo pokazuje da je degradacija potpomognuta svjetlošću mogućnost. Za (110) površinu toplinska karta energija prijenosa elektrona je prikazana na slici 3.9. Vrijednosti između 2.5 eV i 5 eV pokazuju moguću degradaciju potpomognutu svjetlošću za neke pozicije kisika.

5.4 Nazivi slika i tablica na hrvatskom jeziku

Nazivi slika

Nazivi tablica

Bibliography

[1] Aristidou, N.; Eames, C.; Sanchez-Molina, I. et al. Fast oxygen diffusion and iodide defects mediate oxygen-induced degradation of perovskite solar cells // Nature Communications. Vol. 8, 15218 (2017).

[2] Mao, L.; Stoumpos, C. C.; Kanatzidis, M. G. Two-Dimensional Hybrid Halide Perovskites: Principles and Promises // Journal of the American Chemical Society. Vol. 141, 1171-1190 (2019).

[3] Eames, C.; Frost, J. M.; Barnes, P. R. F. et al. Ionic transport in hybrid lead iodide perovskite solar cells // Nature Communications. Vol. 6, 7497 (2015).

[4] Aristidou, N.; Sanchez-Molina, I.; Chotchuangchutchaval, I. et al. The Role of Oxygen in the Degradation of Methylammonium Lead Trihalide Perovskite Photoactive Layers // Angewandte Chemie International Edition. Vol. 54, 8208-8212 (2015).

[5] Ouyang, Y.; Li, Y.; Zhu, P. et al. Photo-oxidative degradation of methylammonium lead iodide perovskite: mechanism and protection // Journal of Materials Chemistry A. Vol. 7, 2275-2282 (2019).

[6] Ouyang, Y.; Shi, L.; Li, Q. et al. Role of Water and Defects in Photo-Oxidative Degradation of Methylammonium Lead Iodide Perovskite // Small Methods. Vol. 3, 1900154 (2019).

[7] Hohenberg, P.; Kohn, W. Inhomogeneous Electron Gas // Physical Review. Vol. 136, B864- B871 (1964).

[8] Kohn, W.; Sham, L. J. Self-Consistent Equations Including Exchange and Correlation Effects // Physical Review. Vol. 140, A1133-A1138 (1965).

[9] Kühne, T. D.; Iannuzzi, M.; Del Ben, M. et al. CP2K: An electronic structure and molecular dynamics software package - Quickstep: Efficient and accurate electronic structure calculations // The Journal of Chemical Physics. Vol. 152, 194103 (2020).

[10] VandeVondele, J.; Hutter, J. An efficient orbital transformation method for electronic structure calculations // The Journal of Chemical Physics. Vol. 118, 4365-4369 (2003).

[11] Weber, V.; VandeVondele, J.; Hutter, J. et al. Direct energy functional minimization under orthogonality constraints // The Journal of Chemical Physics. Vol. 128, 084113 (2008).

[12] Goedecker, S.; Teter, M.; Hutter, J.Separable dual-space Gaussian pseudopotentials // Physical Review B. Vol. 54, 1703-1710 (1996).

[13] VandeVondele, J.; Hutter, J. Gaussian basis sets for accurate calculations on molecular systems in gas and condensed phases // The Journal of Chemical Physics. Vol. 127, 114105 (2007).

[14] Wu, Q.; Van Voorhis, T. Direct optimization method to study constrained systems within density-functional theory // Physical Review A. Vol. 72, 024502 (2005).

[15] Wu, Q.; Van Voorhis, T. Extracting electron transfer coupling elements from constrained density functional theory // The Journal of Chemical Physics. Vol. 125, 164105 (2006).

[16] Becke, A. D. A multicenter numerical integration scheme for polyatomic molecules // The Journal of Chemical Physics. Vol. 88, 2547-2553 (1988).

[17] Hirshfeld, F. L. Bonded-atom fragments for describing molecular charge densities // Theoretica chimica acta. Vol. 44, 129-138 (1977).

[18] Larsen, A. H.; Mortensen, J. J.; Blomqvist, J. et al. The atomic simulation environment—a Python library for working with atoms // Journal of Physics: Condensed Matter. Vol. 29, 273002 (2017).

[19] Smidstrup, S.; Markussen, T.; Vancraeyveld, P. et al. QuantumATK: an integrated platform of electronic and atomic-scale modelling tools // Journal of Physics: Condensed Matter. Vol. 32, 015901 (2019).

[20] Fletcher, R. Practical methods of optimization. 2nd ed. New York : John Wiley & Sons, 1987.

[21] Berland, K.; Hyldgaard, P. Exchange functional that tests the robustness of the plasmon description of the van der Waals density functional // Physical Review B. Vol. 89, 035412 (2014).

[22] Cordon, J. B. Surface Area and Porosity Determinations by Physisorption: Measurement, Classical Theories and Quantum Theory. 1st ed. Elsevier, 2006.

[23] PbI_2 structure CIF, Crystallography Open Database, `https://www.crystallography.net/cod/9009114.html`, 21.9.2022.

[24] Huber, K. P; Herzberg, G. Molecular Spectra and Molecular Structure: IV. Constants of Diatomic Molecules. 1st ed. New York: Springer, 1979.

[25] Lüth, H. Solid Surfaces, Interfaces and Thin Films. 5th ed. Springer, 2010.

[26] Hao, W.; Chen, X.; Li, S. Synergistic Effects of Water and Oxygen Molecule Coadsorption on (001) Surfaces of Tetragonal CH3NH3PbI3: A First-Principles Study // The Journal of Physical Chemistry C. Vol. 120, 28448-28455 (2016).

[27] Gao, X.; Xiangtong, Z.; Yin, W. et al. Ruddlesden–Popper Perovskites: Synthesis and Optical Properties for Optoelectronic Applications // Advanced Science. Vol. 6, 1900941 (2019).

[28] Hunter, J. D. Matplotlib: A 2D graphics environment // Computing in Science & Engineering. Vol. 9, 90-95 (2007).